Supporting Information (SI) for

Titanium isotopes as a tracer for the plume or island arc affinity of felsic rocks

Zhengbin Deng*, Marc Chaussidon, Paul Savage, François Robert, Raphaël Pik, Frédéric Moynier

*Correspondence to: deng@ipgp.fr

This PDF file includes:

Materials and Methods
Supplementary Text
Figs. S1 to S2
References 26-50

Other Supporting Information (SI) for this manuscript includes the following:

Datasets S1 to S8 (separate files)

Materials

Hekla volcanic samples

The Hekla volcanic samples were collected from the flow cores of the historic eruptions of the Hekla volcano, and detailed information on these samples have been published elsewhere (*15*). These rocks cover a compositional range from basaltic to rhyolitic (Dataset S4), and are predominantly aphyric with < 5 % phenocryst contents, which ensure their capability to reflect the melt compositions during magma differentiation. Eleven samples, including two basalt ("HEK05-09" and "HEK12-09"), three basaltic andesite ("HEK-14-09", "HEK17-09" and "HEK21-09"), two andesite ("HEK11-09" and "HEK15-09"), two dacite ("HEK18-9" and "HEK19-09") and two rhyolite ("HEK01-10" and "HEK03-10"), were selected to study their Ti isotopic composition (Dataset S2). The same samples have been previously studied for the stable isotopic compositions of Mo (*26*), Zn (*27*), Si (*15*) and V (*28*). While Mo, Zn and Si have limited isotopic variations over the composition range from basaltic to rhyolitic, V is characterized by a progressive enrichment of the heavy isotope during fractional crystallization of Fe-Ti oxides (≈ 1.5 ‰/amu) (*28*). A similar collection of Hekla samples has been also studied for the Fe isotopic compositions (29): this showed an evolution in two steps for Fe isotopic compositions during magma differentiation, i.e., negligible Fe isotopic variations when SiO_2 = 45-65 wt% and a slight enrichment in the heavy Fe isotopes when SiO_2 > 65 wt%.

www.pnas.org/cgi/doi/10.1073/pnas.1809164115

The studies on the olivine-hosted melt inclusions from the eruptions of Hekla volcano show that, although experiencing some degrees of syn-eruptive degassing, the Hekla magmas are generally volatile-undersaturated before the eruptions, H_2O being the major volatile species (*30*). H_2O behaves as an incompatible component during magma differentiation in the Hekla volcano with H_2O from ≈ 0.80 wt% in the basaltic andesites to ≈ 5.67 wt% in the rhyolites, with a relatively constant H_2O/K_2O ratio of ≈ 2 (*30*, *31*). The estimate for the magma chamber depth using vapor saturation pressures and phenocryst assemblages suggests a crustal magma storage at ≈ 7 km (*30*) and ≈ 6 km (*32*), respectively. Such a crustal magma storage depth at ≈ 6-7 km for the Hekla volcano contrasts with the much shallower magma storage depths for the volcanoes in the Sunda Arc, e.g., Agung (≈ 1.9 km), Sinabung (≈ 0.9 km), Kerinci (≈ 0.7 km), Slamet (≈ 1.2 km), Lawu (≈ 1.1 km), Lamongan (≈ 3.4 km) and Anak Krakatau (≈ 0.7 km) (*33*).

Afar volcanic samples

The Afar samples were collected from the Stratoid Series in the Afar hotspot from East Africa (*16*), including basalt ("AF13-46", "AF13-34" and "AF13-35"), dacite ("AF15-17") and rhyolite ("AF15-40", "AF15-10" and "AF15-11"). These lavas cover the eruption ages ranging between ≈ 4 and ≈ 1 Ma (unpublished data from Pik). The Afar lavas also exhibit the enrichment of TiO_2 during the magma differentiation before the saturation of Fe-Ti oxides. However, in detail the highest TiO_2 content of the Afar lavas is 3.30 wt%, which is much lower than the highest TiO_2 content (4.53 wt%) among the Hekla lavas (Dataset S4). Once the magmas reach the saturation of Fe-Ti oxides, the TiO_2 contents of the magmas decrease with the progressive depletions of total Fe, MgO and CaO (Dataset S4).

Shale samples

The shale samples are from the Canadian Shield and Quebec Appalachians (*34*). Samples "Y-47-83" and "3-05-84" are from the late Archean Gilman Formation and Malartic Group (≈ 2.7 Ga), respectively, in the Abitibi green belt. Sample "85-RG-17-A" is from the mid-Proterozoic Baby Group (≈ 1.8 Ga), Labrador Through. While samples "113", "30" and "43" were collected from the Cambrian to Early Ordovician Magog, St-Roch and Armagh Groups (≈ 0.5 Ga), respectively, samples "PEL 17" and "PEL14" are from the Late Ordovician to Early Silurian Cabano and St-Léon Formations (≈ 0.45 Ga) in the Appalachian Belt (Dataset S3) (*34*).

Banded iron formation (BIF) samples

Sample "sjm/gr/97/21" was a BIF enclave collected from the Amîtsoq gneisses in southern West Greenland (Dataset S3). The gneiss complex from the nearby Akilia Island has been intruded by a metamorphosed quartz-dioritic dike with a zircon U-Pb age of 3,860 ± 10 Ma (*35*, *36*), which confirms the depositional age of the BIF sample in this study at or before ≈ 3.8 Ga.

Chert samples

Sample "2 of 16-09-65" is from the Onverwacht Group, Barberton Greenstone Belt (South Africa) (Dataset S3). The dacitic tuffs of the Onverwacht Group yield the

$^{207}Pb/^{206}Pb$ single zircon evaporation ages between 3,445 ± 3 and 3,416 ± 5 Ma (*37*), implying that sample "2 of 16-09-65" has a deposited age of ≈ 3.5 Ga.

Sample "PPRG 006" was collected from the Warrawoona Formation, Pilbara Block in Western Australia (Dataset S3) (*38*). The dacite in the Warrawoona Formation has a zircon U-Pb age of 3,452 ± 16 Ma (*39*).

Sample "SBO 297" is from the Ventersdorp Supergroup in central South Africa (Dataset S3), which has been previously studied for O isotopic compositions (*40*). The direct dating of the stromatolitic limestones provides an isochron age of 2,557 ± 49 Myrs for the Schmidtsdrif Formation within the Ventersdorp Supergroup (*41*).

Sample "PPRG 226" was collected from the Manjeri Formation, Belingwe Greenstone Belt (Zimbabwe) (Dataset S3) (*42*). The Pb-Pb isochrons from stromatolitic limestones from the Manjeri Formation yield an age of 2,706 ± 49 Ma (*43*).

Methods

Sample preparation and digestion

The rock specimens of the Hekla/Afar volcanic rocks, shales and cherts were washed to remove the soil or organic components. The samples were crushed and further powdered in an agate mill (*15*). Around 30-60 mg of sample powder of Hekla/Afar samples and rock standards (BIR-1, BHVO-2, BCR-2 and AGV-1) were dissolved in the 7 ml Savillex PFA beakers using 2 ml 26 M HF and 1 ml 16 M HNO_3 for overnight cold reaction at room temperature. Afterwards, the samples were dried, and were dissolved in 2 ml 26 M HF and 1 ml 16 M HNO_3 on hot plate at 100 °C for three days. These samples were dried again, and the sample residuals were dissolved in 3 ml 6 M HCl at 130 °C to decompose the fluorides forming during sample digestion by HF. By comparison, around 510-850 mg of powder of chert samples were dissolved following similar protocols but using twice much volumes of 26 M HF and 16 M HNO_3 acids on hot plate at 120 °C for seven days.

The shale samples were dissolved by alkali fusion following the protocol in (*15*) and (*44*). About 17-37 mg of sample powder was fused in Ag crucibles with addition of 200 mg NaOH pellets (99.99 % trace metal basis, Sigma Aldrich Company). The fusion was carried out in a furnace at 720 °C for 15 min, and the fused samples were dissolved in 1 M HNO_3. To ensure that the Ti isotopic measurements of the Hekla samples are not affected by digestion methods, two Hekla samples ("HEK15-09" and "HEK03-10") were digested by alkali fusion to compare with the aliquots dissolved by HF-HNO_3 acids (Dataset S2).

Chromatographic Ti purification

Before the purification of Ti, the sample solutions were mixed with proper amounts of ^{47}Ti-^{49}Ti double spike. The mixture was heated on a hot plate at 100 °C for > 1 h to ensure the homogenization between sample and double spike. The purification of Ti followed a three-steps procedure revised after (*23, 24*): (i) the samples were loaded on a column of 1.1 cm^3 Bio-Rad AG1-X8 resin (200-400 meshes) in 0.5 ml 6 M HCl, and Ti was collected with matrix elements except Fe in 6 ml 6M HCl; (ii) the Ti cut was dissolved in 100 µl 12 M HNO_3, and loaded on a column with 0.2 cm^3 Eichrom DGA resin with particle size of 50-100 µm. Then the matrix elements were washed out by

addition of 900 µl 12 M HNO_3. Subsequently, the Ti was collected by washing with 600 µl MilliQ H_2O and (iii) the Ti cuts from the last step were loaded on the AG1-X8 columns again with 0.5 ml 4 M HF, and the remaining matrix elements were washed out by 9.5 ml 4 M HF. The Ti of the samples was finally collected with additional 5 ml 6 M HCl + 0.01 M HF.

Ti standards and ^{47}Ti-^{49}Ti double spike

A Ti reference material (hereafter expressed as IPGP-Ti) was made from a Ti ICP standard solution (1000 µg/ml PlasmaCal, SCP Science, Lot SC7186430). A ^{47}Ti-^{49}Ti double spike was prepared by mixing enriched ^{47}Ti (95.7 %) and ^{49}Ti (93.3 %), which were purchased from CortecNet (Voisins-le-Bretonneux, France), and was then stored in 1 M HNO_3 + 0.01 M HF. The optimization mixing ratio between sample and double spike was determined using the toolbox from (*45*). The IPGP-Ti and the ^{47}Ti-^{49}Ti double spike were measured separately on mass spectrometer to estimate their Ti isotopic compositions. Cr was doped to determine the instrumental mass bias on Cr isotopes by normalizing to a natural ^{53}Cr/^{52}Cr ratio of 0.1134 (*46*). Once the instrumental $^{50}Cr^+/^{52}Cr^+$ ratio was obtained, the isobaric interferences of $^{50}Cr^+$ on $^{50}Ti^+$ can be corrected through monitoring the intensities of $^{52}Cr^+$ on mass spectrometer. Afterwards, nine aliquots of IPGP-Ti with increasing proportions of double spike were measured. The $\delta^{49}Ti_{IPGP\text{-}Ti}$ value of IPGP-Ti can be preliminarily calculated by conducting double spike inversion for the Ti isotopic data of these mixtures, and the isotopic composition of the ^{47}Ti-^{49}Ti double spike can be further obtained by mass-dependently adapting the calculated $\delta^{49}Ti_{IPGP\text{-}Ti}$ value for IPGP-Ti to 0 ‰. The optimized mixing ratios between IPGP-Ti and double spike were ranging from 0.42 to 0.60 based on the calibration.

Measurements by mass spectrometry, data reduction and results

The Ti cuts were introduced into the Neptune MC-ICP-MS housed at IPGP by using 0.5 M HNO_3 + 0.0015 M HF. An APEX HF desolvating nebulizer (Elemental Scientific Inc., USA) was used to enhance the sensitivity. The typical sensitivities on the MC-ICP-MS were 17-19 V on $^{48}Ti^+$ when using a 10^{11} Ω resistor and a Ti concentration of 300 ppb under medium mass resolution ($M/\Delta M \approx 5800$). The OL-Ti standard was calibrated relative to the IPGP-Ti standard used in (*17*) and (*1*), which provide a $\delta^{49}Ti_{IPGP\text{-}Ti}$ value of -0.140 ± 0.011 ‰ (95 % c.i., n = 8) for IPGP-Ti standard. After each analysis, a washing of the sampling tube and the Apex HF desolvating nebulizer was conducted in two steps, i.e. a first rinse with 1.2 M HNO_3 + 0.0015 M HF and a second rinse with 0.5 M HNO_3 + 0.0015 M HF. Each step of washing contains 50 cycles with an integration time of 8 s, and after the washing the typical background on $^{48}Ti^+$ was 2-5 mV.

The intensities on $^{44}Ca^+$, $^{46}Ti^+$, $^{47}Ti^+$, $^{48}Ti^+$ and $^{49}Ti^+$ were measured simultaneously. Each analysis consisted of 100 cycles with an integration time of 8 s. The intensities on $^{44}Ca^+$ were used to correct the interferences of $^{46}Ca^+$ and $^{48}Ca^+$ on $^{46}Ti^+$ and $^{48}Ti^+$, respectively. Since Ca isotopes can be fractionated on the MC-ICP-MS, the natural Ca isotopic ratios cannot be directly used to correct for the interferences of Ca on Ti. Alternatively, the instrumental Ca isotopic ratios were estimated by mass-dependently fractionate the natural Ca isotopic abundances (^{44}Ca/^{46}Ca = 657.03 and ^{44}Ca/^{48}Ca = 11.14) (*24*) with the instrumental mass fractionation factor of Ti. The estimated instrumental ^{44}Ca/^{46}Ca and ^{44}Ca/^{48}Ca ratios were then applied to correct for the interferences of $^{46}Ca^+$

and $^{48}Ca^{+}$ on $^{46}Ti^{+}$ and $^{48}Ti^{+}$, respectively. Due to the use of a quartz-made injector, there can be also molecular isobaric interferences from silicon oxides and fluorides on the isotopes of Ti, such as $^{28}Si^{16}O^{+}$, $^{30}Si^{16}O^{+}$ and $^{28}Si^{19}F^{+}$. These interferences were avoided by measuring the intensities of $^{44}Ca^{+}$, $^{46}Ti^{+}$ and $^{47}Ti^{+}$ on the lower masses of mass 44, 46 and 47. While the molecular interferences of $^{29}Si^{19}F^{+}$ and $^{30}Si^{19}F^{+}$ on $^{48}Ti^{+}$ and $^{49}Ti^{+}$, respectively, are negligible, the intensities of $^{48}Ti^{+}$ and $^{49}Ti^{+}$ were measured on the central masses of mass 48 and 49.

The data reduction was carried out by using the IsoSpike software developed by (*25*). The intensities of ^{46}Ti, ^{47}Ti, ^{48}Ti and ^{49}Ti after the correction of Ca isobaric interferences were used for double spike inversion to determine the Ti isotopic composition of the samples. The data can be normalized as δ-notation relative to OL-Ti standard:

$$\delta^{49}Ti_{OL-Ti} = \left[\frac{\left({}^{49}Ti / {}^{47}Ti \right)_{sample}}{\left({}^{49}Ti / {}^{47}Ti \right)_{OL-Ti}} - 1 \right] \times 1000 \qquad \text{(Eq. 1)}$$

In order to facilitate data comparison in the community, the present data are reported as $\delta^{49}Ti_{OL\text{-}Ti}$ values, i.e. $\delta^{49}Ti$ if not specifically clarified later. For the rock standards including BHVO-2, BIR-1, BCR-2 and AGV-1, the measurement precisions are the 95 % confidence intervals (95 % c.i.) of three to sixteen duplicates for each sample, which are ≤ 0.022 ‰.

The calibration shows that the IPGP-Ti standard has a $\delta^{49}Ti$ value of +0.140 ± 0.011 ‰ (n = 8). The measurements of a spiked IPGP-Ti aliquot after the DGA pass against the un-cleaned spiked IPGP-Ti provide a systematically resolvable $\Delta^{49}Ti$ value of +0.022 ± 0.009 ‰ (n = 9). This small drift is due to the presence of the highly isotopically fractionated Ca in the used double spike. Since all the samples have been measured against the un-cleaned spiked IPGP-Ti standard, a correction on all the data with error propagation was conducted to take into account this effect, allowing a high-precision inter-laboratory data comparison in the future. After the correction, the $\delta^{49}Ti$ values for rock standards BIR-1, BHVO-2, BCR-2 and AGV-1 are consistent with those reported by (*47*) and (*17*) within errors (Dataset S1). Furthermore, the two alkali fusion aliquots of samples HEK15-09 and HEK03-10 show consistent $\delta^{49}Ti$ values with those of the HF-HNO_3 dissolution aliquots within an analytical precision of 0.030 ‰ (Dataset S2). This consistency implies that the Ti isotopic measurements in this study are not affected by the sample dissolution methods.

Supplementary Text

Mechanisms inducing Ti isotopic variations during magma differentiation

The igneous rocks from both plume and island arc settings become isotopically heavier in Ti with increasing SiO_2 (Fig. 2B). These Ti isotopic variations are intimately associated with the significant decreases of TiO_2 and total Fe (Fig. 2A; Datasets S2 and S4-S5). Such a correlation indicates that the observed Ti isotopic variations here are mainly controlled by the fractional crystallization of Fe-Ti oxides (*17*). Ti is present as 6-folded coordination in Fe-Ti oxides (*48*), while it can be 4-, 5- or 6-fold coordinated in silicate melts (*49*). Given a similar metal-ligand environment (Ti-O), the heavier Ti isotopes would preferentially enter the lower coordinated sites. This predicts that Fe-Ti oxides would be more enriched in the lighter Ti isotopes than silicate melts during

fractional crystallization, and the removal of Fe-Ti oxides leaves behind a residual magma isotopically heavy in Ti.

In this process, two parameters control the evolution of the δ^{49}Ti values of the melt, i.e., the crystal-melt Ti isotopic fractionation factor ($\alpha^{49/47}_{crystal-melt_i_or_j} = R^{49/47}_{crystal} / R^{49/47}_{melt_i_or_j}$ and the fraction of Ti ($f\_Ti_{melt\_j}$ and $f\_Ti_{melt\_i}$) remaining in melt j and melt i compared to the parental melt. The mass balance equation can be written as:

$$R^{49/47}_{melt\_i} = R^{49/47}_{0} \times \left(f\_Ti_{melt\_i}\right)^{\alpha^{49/47}_{crystal-melt\_i}-1} \quad \text{(Eq. 2)}$$

$$R^{49/47}_{melt\_j} = R^{49/47}_{0} \times \left(f\_Ti_{melt\_j}\right)^{\alpha^{49/47}_{crystal-melt\_j}-1} \quad \text{(Eq. 3)}$$

with $R^{49/47}_{0}$, $R^{49/47}_{melt\_i}$ and $R^{49/47}_{melt\_j}$ the ^{49}Ti/^{47}Ti ratios of the parental melt, melt i and melt j, respectively. The isotopic difference between melt j and melt i can be expressed as:

$$\frac{R^{49/47}_{melt\_j}}{R^{49/47}_{melt\_i}} = \frac{\left(f\_Ti_{melt\_j}\right)^{\alpha^{49/47}_{crystal-melt\_j}-1}}{\left(f\_Ti_{melt\_i}\right)^{\alpha^{49/47}_{crystal-melt\_i}-1}} \quad \text{(Eq. 4).}$$

When melt j is compositionally very close to melt i, and melt j and melt i have quite similar liquidus temperatures, $\alpha^{49/47}_{crystal-melt\_j}$ is approximately equal to $\alpha^{49/47}_{crystal-melt\_i}$. As such, Equation 4 can be simplified into:

$$\frac{R^{49/47}_{melt\_j}}{R^{49/47}_{melt\_i}} \approx \left(\frac{f\_Ti_{melt\_j}}{f\_Ti_{melt\_i}}\right)^{\alpha^{49/47}_{crystal-melt\_j}-1} \quad \text{(Eq. 5).}$$

In delta notation, Equation 5 writes:

$$\Delta^{49}Ti_{melt\_j-melt\_i} = \delta^{49}Ti_{melt\_j} - \delta^{49}Ti_{melt\_i} \approx 1000 \times \left(\alpha^{49/47}_{crystal-melt\_j} - 1\right) \times \ln\left(\frac{f\_Ti_{melt\_j}}{f\_Ti_{melt\_i}}\right) \quad \text{(Eq. 6)}$$

The derivation of Equation 6 can provide the instant crystal-melt Ti isotopic fractionation factor $\Delta^{49}Ti_{crystal-melt} = 1000 \times \left(\alpha^{49/47}_{crystal-melt} - 1\right)$. In fact, $f\_Ti_{melt\_j}$ or $f\_Ti_{melt\_i}$ can be estimated by comparing the Ti/Rb ratios of the samples to account for the variations of TiO_2 contents due to fractional crystallization of (i) Ti-free minerals (e.g., olivine and plagioclase) and (ii) Ti-bearing minerals (e.g., pyroxene, ilmenite and titanomagnetite) (see the inset in Fig. 1A) (*14*, *18*). As shown in Fig. S1, the $\Delta^{49}Ti_{crystal-melt}$ can be empirically estimated by making a quadratic regression between the $\delta^{49}Ti_{OL-Ti}$ and $\ln\left(f\_Ti\right)$ values of the Hekla samples. While the temperatures during fractional crystallization of Fe-Ti oxides can be estimated by calculating liquidus temperatures of the samples using rhyolite-MELTS (*50*) with an assumed pre-eruptive $H_2O/K_2O \approx 2$ and a pressure of 2000 bars (*30*), we can compare the $\Delta^{49}Ti_{crystal-melt}$ values with the

temperatures of fractional crystallization. Normally, the $\alpha^{49/47}_{crystal-melt\_i\_or\_j}$ should vary as a function of temperature (T in K) according to:

$\alpha^{49/47}_{crystal-melt\_i\_or\_j} \approx A \times 10^6 / T^2_{melt\_i\_or\_j} + B$ (Eq. 7).

Thus, there should be a linear correlation between the $\Delta^{49}Ti_{crystal-melt}$ and $10^6 / T^2_{melt}$ values if $\alpha^{49/47}_{crystal-melt\_i\_or\_j}$ is only temperature-dependent. However, this is not the case for the Hekla samples, and the coefficients A and B in Equation 7 are not constant. As shown in the inset of Fig. S1, the $\Delta^{49}Ti_{crystal-melt}$ value is increasing with higher $10^6 / T^2_{melt}$ values, but the increase on the $\Delta^{49}Ti_{crystal-melt}$ value gradually slows down when $10^6 / T^2_{melt}$ values are higher. This observation implies that the $\Delta^{49}Ti_{crystal-melt}$ may be not only controlled by the change in temperature but also the change in melt structure, i.e., the stronger melt polymerization with increasing SiO_2 contents that leads to an increase in the fractions of 5- and 4-folded coordinated Ti in the silicate melts (*49*) and enlarges the $\Delta^{49}Ti_{crystal-melt}$ factor. By comparison with the Hekla lavas, the pre-erupted temperatures of the Afar magmas cannot be well estimated yet due to the lack of information on their pre-erupted H_2O contents. However, the similar δ^{49}Ti-SiO_2 paths between the Afar and Hekla samples suggest that Ti isotopes behave similarly in these two igneous suites.

The basaltic to andesitic samples of Agung volcano from Sunda Arc (Dataset S5) (*19*) in (*17*) define a $\Delta^{49}Ti_{crystal-melt}$ value of −0.16 ± 0.01 ‰ (inset in Fig. S1), while the Hekla samples with SiO_2 = 46.5-58.1 wt% show an average value of −0.20 ± 0.01 ‰ (Fig. S1). The $\Delta^{49}Ti_{crystal-melt}$ value provided by the Agung samples agrees with those obtained from the Hekla samples if the Agung H_2O/K_2O ratio is ≈ 0 (i.e., $10^6 / T^2$ = 0.45-0.49), while it would be slightly lower for H_2O/K_2O = 1 or 2 (i.e., $10^6 / T^2$ = 0.48-0.61 or 0.51-0.65, respectively) (see the inset in Fig. S1). This can be probably related to an earlier degassing of H_2O for the Agung volcano due to a shallower magma storage (≈ 1.9 km) (*33*) compared to that of the Hekla volcano (≈ 6-7 km) (*30*, *32*). Alternatively, this small discrepancy in Ti isotopic fractionation could also be due to the fact that in Agung volcano the major Ti-bearing phase fractionated from the melt is titanomagnetite instead of ilmenite in Hekla volcano (Fig. 2A), due to the difference in chemical composition and oxidation state between island arc magmas (calc-alkaline and oxidized) and plume magmas (tholeiitic and reduced).

Despite this slight uncertainty on the Ti-bearing phases fractionated in the various geodynamical settings, it is clear that, at a given SiO_2 content, lavas from plumes show higher δ^{49}Ti values than those from island arcs (Fig. 2B). This isotopic difference is likely the sum of two effects: (i) the lower fO_2 in plume magmas delays the saturation of ilmenite or titanomagnetite, and allows the enrichments of TiO_2 in magmas during olivine and plagioclase accumulation (see the inset in Fig. 1A) (*12*, *18*), and (ii) the higher initial TiO_2 contents in plume magmas allow larger magnitude of depletions of Ti by fractional crystallization of Fe-Ti oxides (Fig. 2A) (*13*).

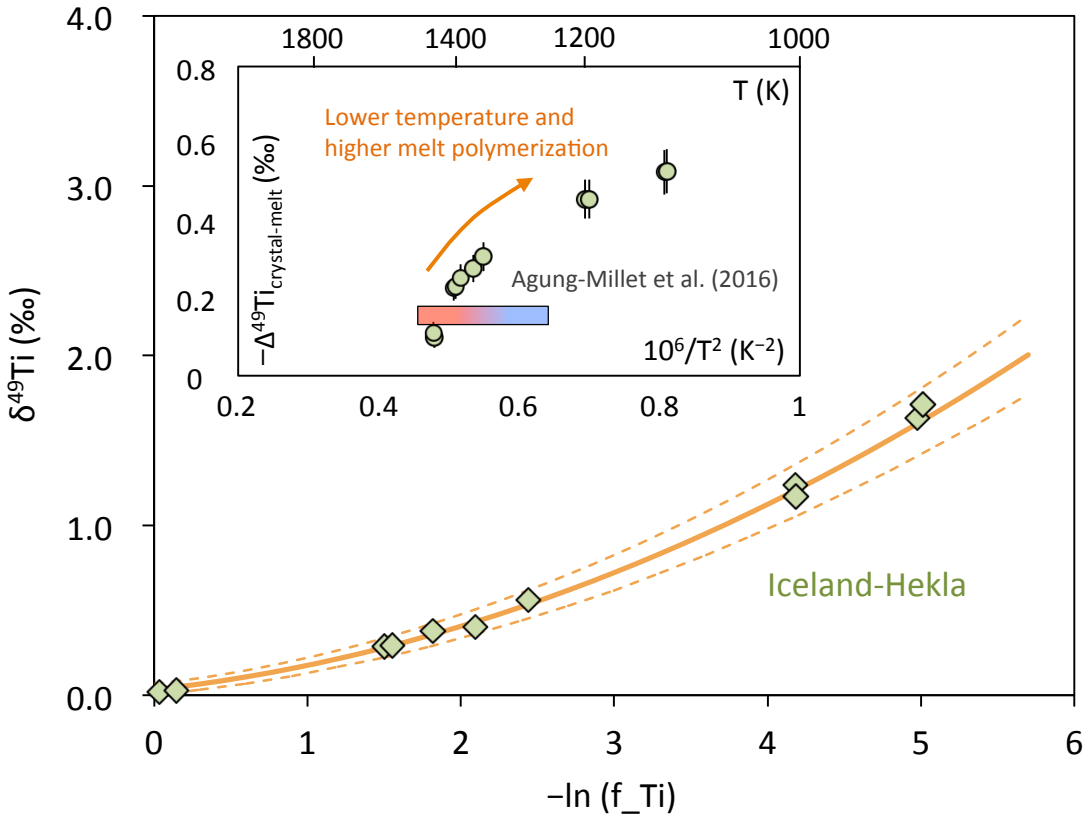

Fig. S1. The correlation between $\delta^{49}Ti$ and $-\ln\left(f\_Ti\right)$ for the Hekla samples. The dashed orange envelope represents the 95 % confidence interval for the regression. The derivation of the quadratic relation between the $\delta^{49}Ti$ and $\ln\left(f\_Ti\right)$ values of the Hekla samples can further provide the instant $\Delta^{49}Ti_{crystal-melt}$ values. The inset shows the relation between the instant $\Delta^{49}Ti_{crystal-melt}$ and $10^6/T^2$ values. The $\Delta^{49}Ti_{crystal-melt}$ value of −0.16 ± 0.01‰ for the Agung basaltic to andesitic samples in (*17*) can be compared with those of the Hekla samples in the inset by using the pre-eruptive H_2O/K_2O ratios of 0 to 2 illustrated by the red to blue change in the colored bar.

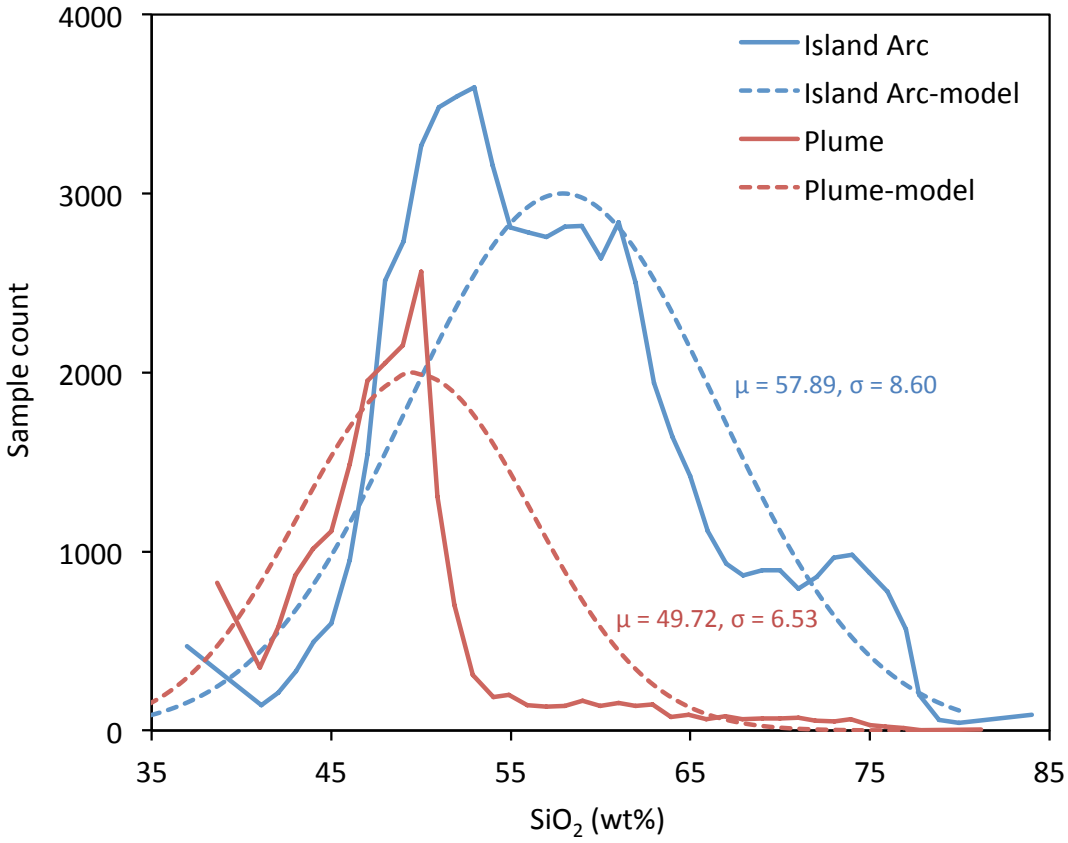

Fig. S2. The SiO_2 distributions for the rocks from plume and island arc settings (the GeoRoc database). Note that some samples may be over-counted due to the non-random sampling, and the SiO_2 distributions for either plume or island arc setting may not strictly follow Gaussian distribution. The use of Gaussian distribution to fit with the dataset provides $\mu = 49.72$ and $\sigma = 6.53$ for the rocks from plume settings ($n = 44{,}089$) while $\mu = 57.89$ and $\sigma = 8.60$ for those from island arc settings ($n = 103{,}090$).

Dataset S1 (separate file)
Ti isotopic compositions of reference materials in this study and literature.
Dataset S2 (separate file)
Ti isotopic compositions of Hekla/Afar volcanic rocks in this study (used in Figs. 2B and S1).
Dataset S3 (separate file)
Ti isotopic compositions of the sedimentary rocks in this study (used in Fig. 3).
Dataset S4 (separate file)
Chemical compositions of Hekla/Afar volcanic rocks and the fractional crystallization modeling results (used in Figs. 1A, 2A-B and S1).
Dataset S5 (separate file)
Chemical compositions of Agung volcanic rocks and the fractional crystallization modeling results (used in Figs. 1A, 2A-B and S1).
Dataset S6 (separate file)
Ti isotopic compositions of the igneous rocks in (*17*) and (*1*) (used in Fig. 2).
Dataset S7 (separate file)
Ti isotopic compositions of the individual and composite shale samples in (*1*) (used in Fig. 3).
Dataset S8 (separate file)
The literature TiO_2 contents of shales, cherts and BIFs (used in the inset in Fig. 3).

References

1. Greber ND *et al.* (2017) Titanium isotopic evidence for felsic crust and plate tectonics 3.5 billion years ago. *Science* **357**: 1271–1274. doi: 10.1126/science.aan8086
2. Korenaga J (2013) Initiation and evolution of plate tectonics on Earth: theories and observations. *Annu. Rev. Earth Planet. Sci.* **41**: 117–151. doi: 10.1146/annurev-earth-050212-124208
3. Watson EB, Harrison TM (2005) Zircon thermometer reveals minimum melting conditions on earliest Earth. *Science* **308**: 841–844. doi: 10.1126/science.1110873
4. Martin H (1986) Effect of steeper Archean geothermal gradient on geochemistry of subduction-zone magmas. *Geology* **14**: 753–756. doi: 10.1130/0091-7613(1986)14<753:EOSAGG>2.0.CO;2
5. Dhuime B, Wuestefeld A, Hawkesworth CJ (2015) Emergence of modern continental crust about 3 billion years ago. *Nat. Geosci.* **8**: 552−555. doi: 10.1038/ngeo2466
6. Tang M, Chen K, Rudnick RL (2016) Archean upper crust transition from mafic to felsic marks the onset of plate tectonics. *Science* **351**: 372−375. doi: 10.1126/science.aad5513
7. Harrison TM, Bell EA and Boehnke P (2017) Hadean zircon petrochronology. *Rev. Mineral. Geochem.* **83**: 329–363. doi: 10.2138/rmg.2017.83.11
8. Boehnke P, Bell EA, Stephan T, Trappitsch R, Keller CB, Pardo OS, Davis AM, Harrison TM, Pellin MJ (2018) Potassic, high-silica Hadean crust. *Proc. Natl. Acad. Sci. USA*, p.201720880. doi: 10.1073/pnas.1720880115
9. Campbell IH, Davies DR (2017) Raising the continental crust. *Earth Planet. Sci. Lett.* **460**: 112–122. doi: 10.1016/j.epsl.2016.12.011
10. Reimink JR, Chacko T, Stern RA, Heaman LM (2014) Earth's earliest evolved crust generated in an Iceland-like setting. *Nat. Geosci.* **7**: 529–533. doi: 10.1038/ngeo2170
11. Willbold M, Hegner E, Stracke A, Rocholl A (2009) Continental geochemical signatures in dacites from Iceland and implications for models of early Archaean crust formation. *Earth Planet. Sci. Lett.* **279**: 44–52. doi: 10.1016/j.epsl.2008.12.029
12. Toplis MJ, Carroll MR (1995) An experimental study of the influence of oxygen fugacity on Fe-Ti oxide stability, phase relations, and mineral-melt equilibria in ferro-basaltic systems. *J. Petrol.* **36**: 1137–1170. doi: 10.1093/petrology/36.5.1137
13. Cawthorn RG, Biggar GM (1993) Crystallization of titaniferous chromite, magnesian ilmenite and armalcolite in tholeiitic suites in the Karoo Igneous Province. *Contrib. Mineral. Petrol.* **114**: 221–235. doi: 10.1007/BF00307757
14. Nandedkar RH, Ulmer P, Müntener O (2014) Fractional crystallization of primitive, hydrous arc magmas: an experimental study at 0.7 GPa. *Contrib. Mineral. Petrol.* **167**: 1015. doi: 10.1007/s00410-014-1015-5
15. Savage PS, Georg RB, Williams HM, Burton KW, Halliday AN (2011) Silicon isotope fractionation during magmatic differentiation. *Geochim. Cosmochim. Acta*. **75**: 6124–6139. doi: 10.1016/j.gca.2011.07.043
16. Pik R, Marty B, Hilton DR (2005) How many mantle plumes in Africa? The geochemical point of view. *Chem. Geol.* **226**: 100–114. doi: 10.1016/j.chemgeo.2005.09.016

17. Millet MA, Dauphas N, Greber ND, Burton KW, Dale CW, Debret B, Macpherson CG, Nowell GM, Williams HM (2016) Titanium stable isotope investigation of magmatic processes on the Earth and Moon. *Earth Planet. Sci. Lett.* **449**: 197–205. doi: 10.1016/j.epsl.2016.05.039
18. Prytulak J, Elliott T (2007) TiO_2 enrichment in ocean island basalts. *Earth Planet. Sci. Lett.* **263**: 388–403. doi: 10.1016/j.epsl.2007.09.015
19. Dempsey S (2013) Geochemistry of volcanic rocks from the Sunda Arc. *Doctoral thesis*, Durham University.
20. Keller CB, Schoene B (2012) Statistical geochemistry reveals disruption in secular lithospheric evolution about 2.5 Gyr ago. *Nature* **485**: 490–493. doi: 10.1038/nature11024
21. Deng Z, Moynier F, Sossi PA, Chaussidon M (in press) Bridging the depleted MORB mantle and the continental crust using titanium isotopes. *Geochem. Perspect. Lett.*
22. Rudnick RL, Gao S (2003) Composition of the continental crust. *Treatise on Geochemistry* **3**: 659. doi: 10.1016/B0-08-043751-6/03016-4
23. Deng Z, Moynier F, van Zuilen K, Sossi PA, Pringle EA, Chaussidon M (2018) Lack of resolvable titanium stable isotopic variations in bulk chondrites. *Geochim. Cosmochim. Acta*. **239**: 409–419. doi: 10.1016/j.gca.2018.06.016
24. Zhang J, Dauphas N, Davis AM, Pourmand A (2011) A new method for MC-ICPMS measurement of titanium isotopic composition: Identification of correlated isotope anomalies in meteorites. *J. Anal. At. Spectrom.* **26**: 2197–2205. doi: 10.1039/C1JA10181A
25. Creech JB, Paul B (2015) IsoSpike: Improved Double‐Spike Inversion Software. *Geostand. Geoanal. Res.* **39**: 7−15. doi: 10.1111/ j.1751-908X.2014.00276.x
26. Yang J, Siebert C, Barling J, Savage P, Liang YH, Halliday AN (2015) Absence of molybdenum isotope fractionation during magmatic differentiation at Hekla volcano, Iceland. *Geochim. Cosmochim. Acta.* **162**: 126–136. doi: 10.1016/j.gca.2015.04.011
27. Chen H, Savage PS, Teng FZ, Helz RT, Moynier F (2013) Zinc isotope fractionation during magmatic differentiation and the isotopic composition of the bulk Earth. *Earth Planet. Sci. Lett.* **369–370**: 34–42. doi: 10.1016/j.epsl.2013.02.037
28. Prytulak J, Sossi PA, Halliday AN, Plank T, Savage PS, Woodhead JD (2017) Stable vanadium isotopes as a redox proxy in magmatic systems? *Geochem. Perspect. Lett.* **3**: 75–84. doi: 10.7185/geochemlet.1708
29. Schuessler JA, Schoenberg R, Sigmarsson O (2009) Iron and lithium isotope systematics of the Hekla volcano, Iceland-Evidence for Fe isotope fractionation during magma differentiation. *Chem. Geol.* **258**: 78–91. doi: 10.1016/j.chemgeo.2008.06.021
30. Lucic G, Berg AS, Stix J (2016) Water-rich and volatile-undersaturated magmas at Hekla volcano, Iceland. *Geochem. Geophys. Geosyst.* **17**: 3111–3130. doi: 10.1002/2016GC006336
31. Moune S, Sigmarsson O, Thordarson T, Gauthier PJ (2007) Recent volatile evolution in the magmatic system of Hekla volcano, Iceland. *Earth Planet. Sci. Lett.* **255**: 373–389. doi: 10.1016/j.epsl.2006.12.024

32. Weber G, Castro JM (2017) Phase petrology reveals shallow magma storage prior to large explosive silicic eruptions at Hekla volcano, Iceland. *Earth Planet. Sci. Lett.* **466**: 168–180. doi: 10.1016/j.epsl.2017.03.015
33. Chaussard E, Amelung F (2012) Precursory inflation of shallow magma reservoirs at west Sunda volcanoes detected by InSAR. *Geophys. Res. Lett.* **39**. doi:10.1029/2012GL053817
34. Dia A, Dupre B, Gariepy C, Allegre CJ (1990) Sm-Nd and trace-element characterization of shales from the Abitibi Belt, Labrador Trough, and Appalachian Belt: consequences for crustal evolution through time. *Can. J. Earth Sci.* **27**: 758–766. doi: 10.1139/e90-077
35. Mojzsis SJ, Arrhenius G, McKeegan KD, Harrison TM, Nutman AP, Friend CRL (1996) Evidence for life on Earth before 3,800 million years ago. *Nature* **384**: 55–59. doi: 10.1038/384055a0
36. Nutman AP, McGregor VR, Friend CRL, Bennett VC, Kinny PD (1996) The Itsaq Gneiss Complex of southern West Greenland; the world's most extensive record of early crustal evolution (3900-3600 Ma). *Precambrian Res.* **78**: 1–39. doi: 10.1016/0301-9268(95)00066-6
37. Krüner A, Byerly GR, Lowe DR (1991) Chronology of early Archaean granite-greenstone evolution in the Barberton Mountain Land, South Africa, based on precise dating by single zircon evaporation. *Earth Planet. Sci. Lett.* **103**: 41–54. doi: 10.1016/0012-821X(91)90148-B
38. Schopf JW (1983) Earth's earliest biosphere: its origin and evolution. Princeton University Press, Princeton, NJ, USA.
39. Pidgeon RT (1978) 3450-m.y.-old volcanics in the Archaean layered greenstone succession of the Pilbara Block, Western Australia. *Earth Planet. Sci. Lett.* **37**: 421–428. doi: 10.1016/0012-821X(78)90057-2
40. Beaumont V, Robert F (1999) Nitrogen isotope ratios of kerogens in Precambrian cherts: A record of the evolution of atmosphere chemistry? *Precambrian Res.* **96**: 63–82. doi: 10.1016/S0301-9268(99)00005-4
41. Jahn B, Bertrand-Sarfati J, Morin N, Mace J (1990) Direct dating of stromatolitic carbonates from the Schmidtsdrif Formation (Transvaal Dolomite), South Africa, with implications on the age of the Ventersdorp Supergroup. *Geology* **18**: 1211–1214. doi: 10.1130/0091-7613(1990)018<1211:DDOSCF>2.3.CO;2
42. Karhu J, Epstein S (1986) The implication of the oxygen isotope records in coexisting cherts and phosphates. *Geochim. Cosmochim. Acta.* **50**: 1745–1756. doi: 10.1016/0016-7037(86)90136-5
43. Bolhar R, Hofmann A, Woodhead J, Hergt J, Dirks P (2002) Pb- and Nd-isotope systematics of stromatolitic limestones from the 2.7 Ga Ngezi group of the Belingwe Greenstone Belt: Constraints on timing of deposition and provenance. *Precambrian Res.* **114**: 277–294. doi: 10.1016/S0301-9268(01)00229-7
44. Pringle EA, Savage PS, Jackson MG, Barrat JA, Moynier F (2013) Si isotope homogeneity of the solar nebula. *Astrophys. J.* **779**. doi:10.1088/0004-637X/779/2/123.
45. Rudge JF, Reynolds BC, Bourdon B (2009) The double spike toolbox. *Chem. Geol.* **265**: 420–431. doi: 10.1016/j.chemgeo.2009.05.010

46. de Laeter JR, Böhlke JK, De Bièvre P, Hidaka H, Peiser HS, Rosman KJR, Taylor PDP (2003) Atomic weights of the elements. Review 2000 (IUPAC Technical Report). *Pure Appl. Chem.* **75**, doi:10.1351/pac200375060683.
47. Williams N. H. (2014) Titanium isotope cosmochemistry. Ph.D. thesis, Manchester Univ.
48. Papike JJ, Karner JM, Shearer CK (2005) Comparative planetary mineralogy: Valence state partitioning of Cr, Fe, Ti, and V among crystallographic sites in olivine, pyroxene, and spinel from planetary basalts. *Am. Mineral.* **90**: 277–290. doi: 10.2138/am.2005.1779
49. Farges F, Brown GE (1997) Coordination chemistry of titanium(IV) in silicate glasses and melts: IV. XANES studies of synthetic and natural volcanic glasses and tektites at ambient temperature and pressure. *Geochim. Cosmochim. Acta.* **61**: 1863–1870. doi: 10.1016/S0016-7037(97)00050-1
50. Gualda GAR, Ghiorso MS, Lemons RV, Carley TL (2012) Rhyolite-MELTS: A modified calibration of MELTS optimized for silica-rich, fluid-bearing magmatic systems. *J. Petrol.* **53**: 875–890. doi: 10.1093/petrology/egr080